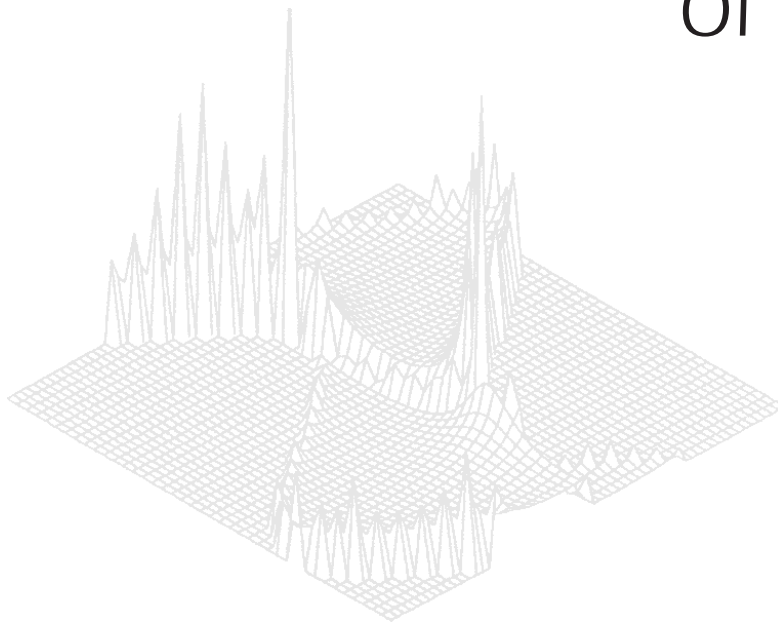

C S I R O P U B L I S H I N G

Australian Journal of Physics

Volume 51, 1998
© CSIRO 1998



A journal for the publication of
original research in all branches of physics

www.publish.csiro.au/journals/ajp

All enquiries and manuscripts should be directed to

Australian Journal of Physics

CSIRO PUBLISHING

PO Box 1139 (150 Oxford St)

Collingwood

Vic. 3066

Australia

Telephone: 61 3 9662 7626

Facsimile: 61 3 9662 7611

Email: peter.robertson@publish.csiro.au



Published by **CSIRO PUBLISHING**
for CSIRO and the
Australian Academy of Science



MAPON Spectroscopy and Its Application to Transition Metal Ferromagnets*

W. D. Hutchison, N. Yazidjoglou^A and D. H. Chaplin

School of Physics, University College,
University of New South Wales, Australian Defence Force Academy,
Canberra, ACT 2600, Australia.

^A Present address: ANUTech Pty Ltd,
Canberra, ACT 0200, Australia.

Abstract

Modulated adiabatic passage on oriented nuclei (MAPON) is a technique developed specifically to measure very small electric quadrupole interactions (EQIs) at radioactive probe nuclei even when such interactions are masked in the frequency domain by inhomogeneous magnetic broadening associated with a dominant magnetic hyperfine interaction. In this paper an overview of the technique is presented with particular reference to ⁶⁰CoCo EQI measurements which were an important step in establishing MAPON methodology. MAPON results for dilute and impurities in ferromagnetic Fe and Ni metal hosts are reviewed including presentation of new data for ⁵⁸CoNi and ⁶⁰CoNi. Priorities for future studies are provided on the basis of this review.

1. Introduction

Modulated adiabatic passage on oriented nuclei (MAPON), a transient nuclear magnetic resonance on oriented nuclei (NMRON) technique, has now been in use at ADFA for over a decade. The technique was developed by the Canberra NMRON group in collaboration with Professor Paul Callaghan of Massey University specifically to measure very small electric quadrupole interactions (EQIs) of oriented probe nuclei, even when such effects are masked in the frequency domain by inhomogeneous magnetic broadening associated with a dominant magnetic hyperfine interaction (Callaghan *et al.* 1985, 1988). This is a common circumstance for light-to-intermediate mass probe nuclei ($A < 150$) placed substitutionally in the conventional nuclear orientation hosts, Fe, Ni and Co. MAPON spectroscopy, which has excellent combined sensitivity and absolute energy resolution, the latter approaching 100 Hz, is currently without peer as a technique for measuring small EQIs and therefore, in principle, electric field gradients (EFGs) and excited state quadrupole moments. Indeed both EFGs (Co in single crystal Fe) and an excited state quadrupole moment (⁵⁶Co) were obtained in the original experimental papers for the CoFe system (Back *et al.* 1988; Back 1988). In recent years MAPON has been found useful by other groups, e.g. Hagn (1996) and Herzog (1996), for making similar measurements. Hagn (1996) has commented specifically on

* Refereed paper based on a contribution to the International Workshop on Nuclear Methods in Magnetism, held in Canberra on 21–23 July 1997.

the utilitarian role of the hcp Co host in measurements of excited state nuclear quadrupole moments.

This paper presents an overview of MAPON spectroscopy with particular reference to $^{60}\text{CoCo}$ EQI measurements (Hutchison *et al.* 1991, 1992*a*) which were an integral part of establishing the credentials of MAPON spectroscopy and in part led to the above wider interest in the technique. Specifically, the measurement of the EQI at the ^{60}Co site in hexagonal (hcp) cobalt not only enabled the first direct quantitative verification of MAPON data against a proven technique, conventional NMR, but also demonstrated the applicability of MAPON measurements to the larger EQI values encountered with hcp cobalt hosts. This also implies the applicability of MAPON to heavier impurities in crystallographically cubic hosts such as Fe and Ni without the need for the extreme care in sample preparation required to frequency resolve quadrupolar split lines in QI NMRON (Hinfurtner *et al.* 1991; Hagn 1996). Apart from the measurements on elemental cobalt, together with work on brute force oriented elemental silver (Hutchison *et al.* 1992*b*), studies by the Canberra NMRON group have concentrated on impurity probes in ferromagnetic Fe and Ni metal hosts and this set of results is supplemented with the presentation of new data for $^{58}\text{CoNi}$ and $^{60}\text{CoNi}$.

2. MAPON Spectroscopy

MAPON, together with the parent technique of adiabatic fast (single) passage (Don 1972; Callaghan *et al.* 1974) and pulsed NMRON (see Chaplin and Wilson 1986), are examples of techniques referred to as transient methods in NMRON. For these methods the basic underlying principle is the same as for the more widely practised continuous wave (CW) NMRON in that magnetic resonance is performed on thermally oriented radioactive nuclei and detection is via the measurement of the variation in the anisotropic distribution of nuclear radiation (normally γ -ray) occurring as a result of a resonant radio-frequency (RF) field changing the nuclear Zeeman populations. The essential difference in the transient case is that the experiment moves from the frequency to the time domain just as with CW NMR versus pulsed NMR.

(2a) Low Temperature Nuclear Orientation

The first step in any NMRON experiment is to obtain a reasonable degree of low temperature nuclear orientation (LTNO) resulting in some anisotropy in the emission of γ -radiation from the ensemble of radioactive probe nuclei. The usual method is to incorporate the probe nuclei by thermal or implantation means into a ferromagnetic metal. Even with the probe nucleus then experiencing a hyperfine field of typically several tens of tesla, very low temperatures (~ 10 mK) are usually required. The angular distribution for gamma radiation from an oriented nuclear ensemble is given by

$$W(\theta) = 1 + B_2 U_2 A_2 P_2(\cos\theta) + B_4 U_4 A_4 P_4(\cos\theta), \quad (1)$$

where θ is the angle between the direction of detection and the magnetic field at the nucleus, U_λ are nuclear de-orientation coefficients, A_λ are angular distribution coefficients and P_λ are Legendre polynomials. The B_λ are the orientation parameters which, for host systems with a dominant magnetic hyperfine interaction such as

Fe, Ni or Co, reflect the nuclear Zeeman populations of the probe with nuclear spin I . Then

$$B_\lambda = [(2\lambda + 1)(2I + 1)]^{\frac{1}{2}} \sum_{m=-I}^I \begin{pmatrix} I & I & \lambda \\ -m & m & 0 \end{pmatrix} p(m), \quad (2)$$

where the populations $p(m)$ assumed in thermal equilibrium are governed by the Boltzmann distribution:

$$p(m) = \exp\left(-\frac{m\mu B}{IkT}\right) / \sum_{m=-I}^I \exp\left(-\frac{m\mu B}{IkT}\right). \quad (3)$$

Here μ is the nuclear magnetic dipole moment of the probe nucleus and B is the effective magnetic field at the nucleus, which for the ferromagnetic host will usually be of the order of the magnetic hyperfine field. A schematic showing the angular distribution derived from equation (1) for $^{60}\text{CoFe}$ ($I = 5$, $\mu = +3.79$ nm and $|B_{\text{hyp}}| = 29$ T) is illustrated in Fig. 1.

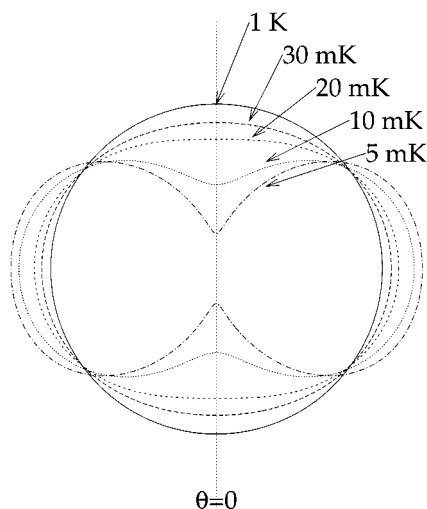


Fig. 1. Schematic diagram of the angular distribution of γ -ray emission for low temperature nuclear orientation of $^{60}\text{CoFe}$.

(2b) NMRON

The development of NMRON (Mathias and Holliday 1966) combined the spectroscopic accuracy of NMR with the sensitivity derived from LTNO. The NMRON technique is conceptually straight forward; resonant RF perturbs the oriented nuclear substate populations, resulting in an observed change in gamma-ray counts into a fixed detector. In the CW technique the measurement proceeds via monitoring gamma-ray counts from the oriented ensemble as a function of RF frequency. Frequency modulation (FM) is required in the case of a dilute spin system with inhomogeneous magnetic broadening to generate sufficient signal. Indeed in this case ‘FM off’ is generally used to establish the non-resonant base line level, which may vary significantly over several MHz reflecting RF

cable response to an inevitably mismatched electrical load. As an example, CW NMRON of $^{60}\text{CoNi}$ can be seen in Fig. 2.

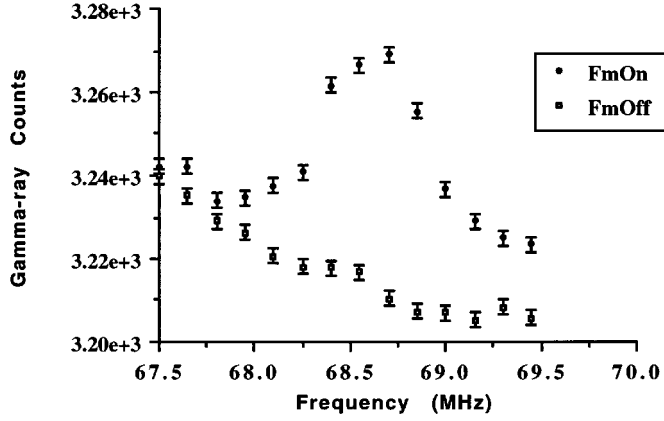


Fig. 2. Resonance spectra of $^{60}\text{CoNi}$ (1) along the $\langle 111 \rangle$ easy axis at $B_{\text{app}} = 0.15$ T, obtained via CW NMRON with 400 Hz triangular modulation frequency, an FM amplitude of ± 200 kHz and $V_{\text{RF}} = 1$ dBm.

(2c) Transient Methods in NMRON

Single Passage. In transient NMRON a pulse or burst of resonant RF is applied and any change in γ -ray anisotropy with subsequent return to equilibrium is recorded. The technique of adiabatic fast (or single) passage where the RF is swept through the line in a time fast compared to relaxation times is an example of transient NMRON (see Fig. 4 where a single passage of duration 147 ms is applied at the 50 s mark).

If the nuclear ensemble experiences purely an axial magnetic Zeeman interaction, the single passage experiment would produce population inversion. However, in practice, even in nominally cubic hosts, for probe nuclei with $I \geq 1$ a small electric quadrupole term usually exists, perturbative to the dominant magnetic (hyperfine) interaction:

$$H = -g\mu_{\text{N}} B I_z + P \left[I_z^2 - \frac{1}{3} I(I+1) \right], \quad (4)$$

where

$$P = \frac{3eV_{zz}Q}{4I(2I-1)} P_2(\cos\alpha),$$

and for simplicity it has been assumed that the EQI is axially symmetric, V_{zz} is the principal electric field gradient (EFG) at the nucleus, Q is the nuclear quadrupole moment and α is the angle between V_{zz} and the magnetic field

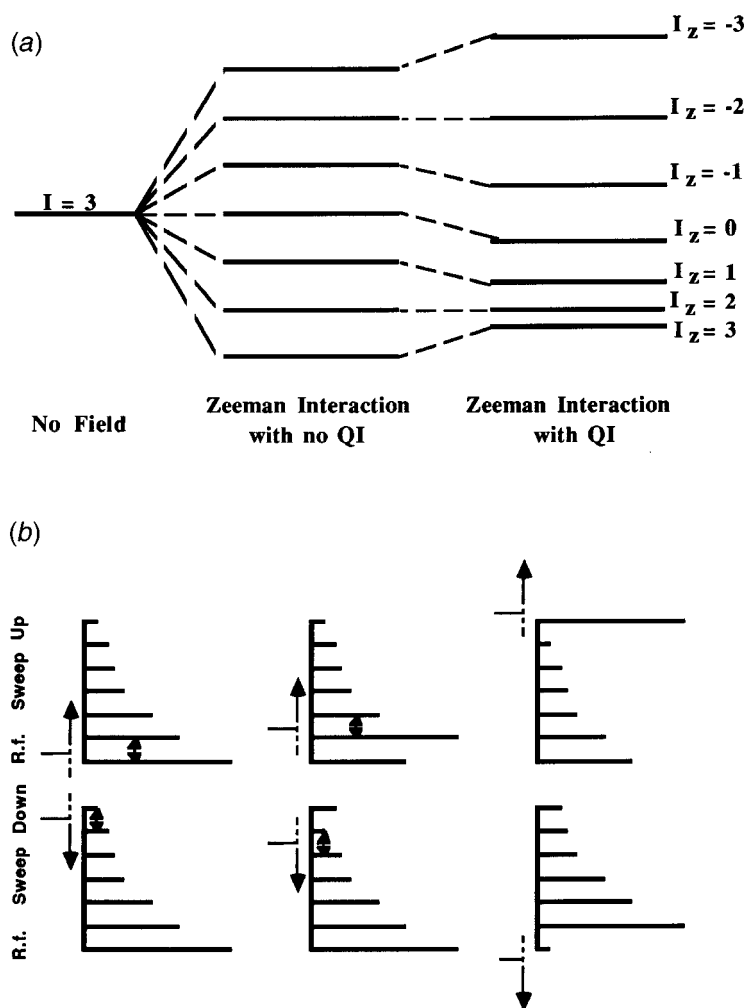


Fig. 3. (a) Zeeman splitting for an $I = 3$ nuclear spin system into $2I+1$ substates and the effect of a small positive electric quadrupole interaction on these energy levels (note the scale of the EQI is grossly exaggerated since, in nominally cubic hosts, the EQI is many orders of magnitude smaller than the Zeeman term). (b) Successive cyclic inversion of the adjacent sublevel populations via an adiabatic fast (single) passage, resulting in a cyclic shift of populations and a post-passage population distribution dependent on sweep direction (after Yazidjoglou 1989). The ordinate scale is such that the inequality in the energy level splitting is not apparent, but the differences between these levels are nevertheless greater than the RF Zeeman term.

B. As an example, an energy level diagram appropriate to the Hamiltonian of equation (4) is depicted in Fig. 3a for a spin 3 nuclear ensemble. The effect of the small quadrupolar term is to lift the degeneracy within the nuclear Zeeman manifold. Therefore, a single passage applied to this nuclear ensemble will cause cyclic permutation of the adjacent Zeeman substate populations as depicted in Fig. 3b. The resulting population configuration, and hence the non-equilibrium gamma anisotropy will be dependent on whether the RF sweep enters the least

or most populated substate first. In turn the actual sweep direction, up or down, corresponding to entering the least or most populated substate first depends solely on the sign of P , therefore enabling a determination of the sign of the EQI from the observed sweep asymmetry (Callaghan *et al.* 1974). This point is illustrated in Fig. 4 where single passage measurements for a $^{60}\text{CoCo}$ hcp single crystal are shown. Here the EQI is intrinsically negative for the magnetisation along the c -axis ($\alpha = 0$) but becomes effectively positive when the magnetisation is forced perpendicular to the c -axis ($\alpha = \pi/2$) with an applied field; this change is seen via the reversal of the sweep asymmetry of the post passage signals.

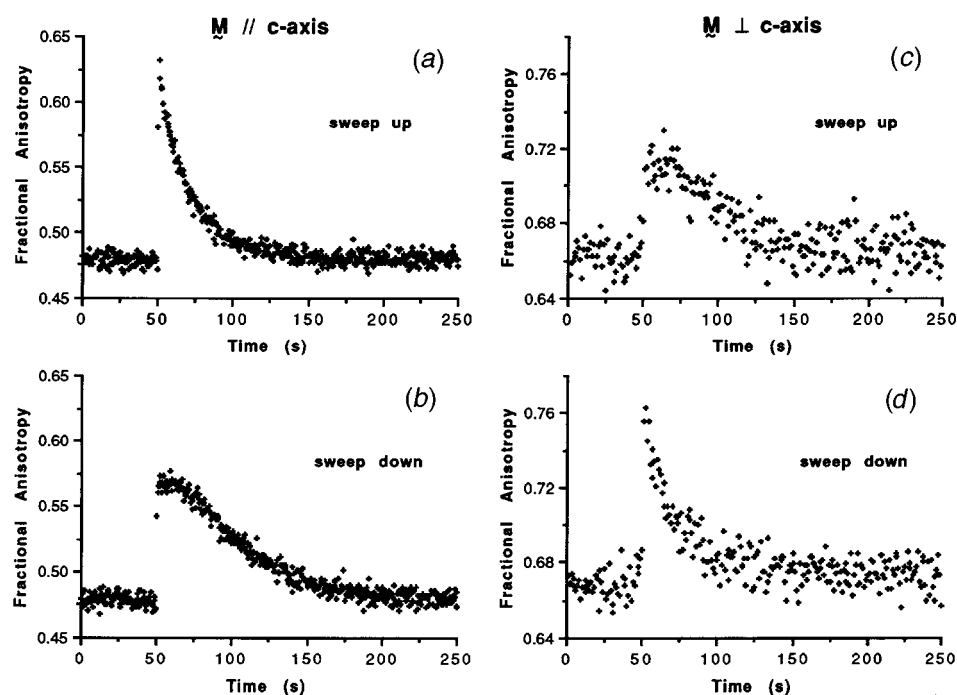


Fig. 4. Single passage NMRON relaxation curves for a $^{60}\text{CoCo}$ hcp single crystal illustrating the change in the sign of EQI from negative when the magnetisation is parallel to the c -axis to positive when in the basal plane (after Hutchison *et al.* 1992a). Parts (a) and (b) are signals obtained in zero applied field with gamma detection parallel to the c -axis, for sweep up and down respectively. Parts (c) and (d) were obtained with field 1.6 T applied perpendicular to the c -axis, to rotate the magnetisation to be orthogonal with the principal EFG axis.

MAPON. In modulated adiabatic passage the swept single frequency used above is replaced by a signal where the RF carrier is modulated at a frequency f_m . This is achieved with a double balance mixer resulting in a double side-band, suppressed carrier, RF spectrum. A typical MAPON RF signal is shown in Fig. 5. To a good approximation this spectrum consists of two RF peaks separated by $2f_m$. When such a signal is swept through the nuclear ensemble, with perturbative EQI, the resulting post passage change in anisotropy will depend

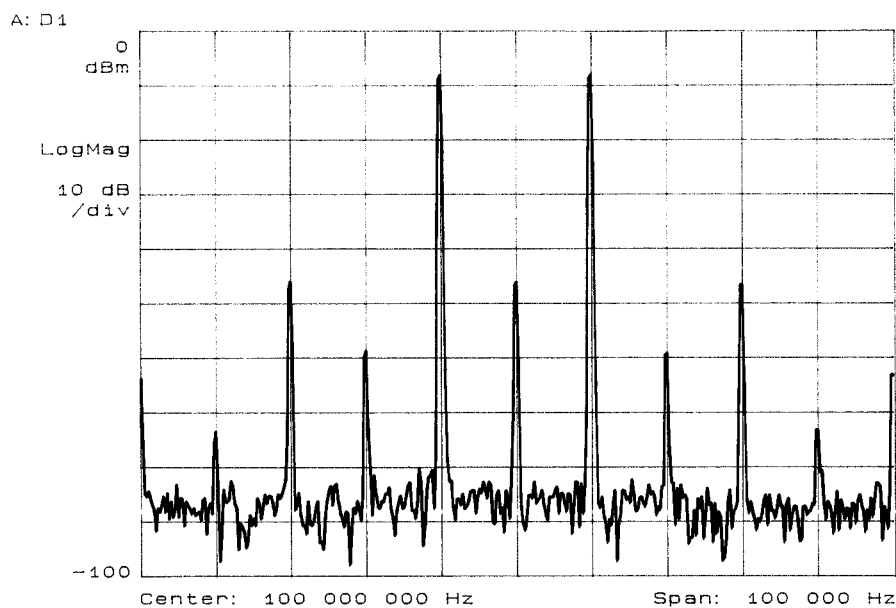


Fig. 5. Double side-band suppressed carrier frequency spectrum of a typical MAPON RF signal display on a spectrum analyser. Note that the vertical scale is logarithmic, with the carrier and second harmonics suppressed by approximately 38 dB.

on the extent of the modulation f_m compared to the magnitude of the EQI, P/h . Therefore, the modulation f_m is the key variable of MAPON spectroscopy. If $f_m \ll P/h$, the MAPON passage can be thought of as two sequential single passages, the latter passage undoing the effects of the first, leaving the substate populations unaltered. If, however, $f_m \gg P/h$ then a MAPON passage will move two first-entered populations successively through the ensemble, in general causing a large change in post passage anisotropy particularly when the sweep direction corresponds to entering least populated states first. The scenario for both these cases is depicted in Fig. 6. A large increase in post passage signal is expected when $f_m = P/h$. This point is illustrated by the raw (or integral) MAPON data for hcp $^{60}\text{CoCo}$ shown in Fig. 7a. Of course, in practice, many systems will have non-unique distributions of P values, and in this case the differential of the raw MAPON data will be representative of the EQI distribution. Fig. 7b shows the differential MAPON spectra for $^{60}\text{CoCo}$ in both cubic and hexagonal specimens. This marked difference in EQI mode values is in striking contrast to the magnetic hyperfine interactions which differ by only $\sim 2\%$ between the two phases of cobalt metal. In Fig. 7b the different frequency distributions compare the lattice dominated (more unique) EQI of the hexagonal lattice with the broader and smaller local moment generated EQI in the cubic case. Furthermore, from these elemental cobalt MAPON results two significant conclusions were drawn:

- (i) From the mode EQI value of $P/h = -48.5(5)$ kHz for $^{60}\text{CoCo}$ hcp measured with MAPON, an EFG value can be determined and comparison made with the result of Fekete *et al.* (1978) for ^{59}Co spin echo NMR. The EFG determinations from the two techniques are found to be in excellent agreement.

- (ii) The fcc cobalt mode EQI of $P/h = -6.2(4)$ kHz equates well to the isotropic relativistic (or local moment) component assigned as part of the total hcp EFG by Fekete *et al.* (1978). Indeed the MAPON results for this elemental system show internal consistency for the additivity of the lattice EFG and the local moment EFG. Explicitly for hcp Co we have $P_{\text{total}} = P_{\text{RQI}} + P_{\text{lat}}P_2(\cos\alpha)$. For B parallel to the c -axis, $P_{\text{total}}/h = -48.5(5)$ kHz and using $P_{\text{RQI}}/h = P_{\text{fcc}}/h = -6.2(4)$ kHz we calculate $P_{\text{lat}}/h = -42.3(7)$ kHz. While with B perpendicular to the c -axis, $P_{\text{total}}/h = +14.9(3)$ kHz leading to $P_{\text{lat}}/h = -42.2(5)$ kHz. Note that the EQI values used here are taken from Table 1 of Hutchison *et al.* (1992a). The values for fcc Co and hcp with M in the basal plane have been incorrectly transcribed to Table 2 of Chaplin and Hutchison (1992).

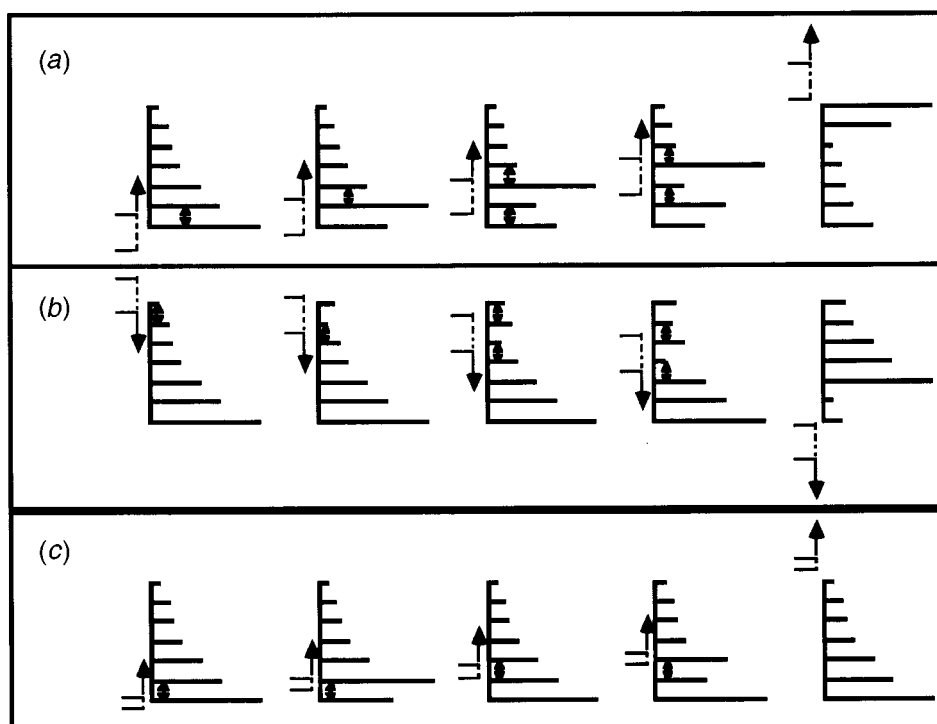


Fig. 6. Parts (a) and (b) show the evolution of Zeeman populations during a modulated adiabatic passage on quadrupolar split levels with the RF entering the most and least populated levels first, respectively, for the case when $f_m \gg P/h$. Part (c) shows the case of RF entering the most populated level first when $f_m \ll P/h$ (after Yazidjoglou 1989). The ordinate scale is such that the inequality in the energy level splitting is not apparent, but the differences between these levels are nevertheless greater than the RF Zeeman term.

In this section a brief outline of the MAPON technique has been presented. It should be noted that the technique applies to nuclear ensembles where the magnetic inhomogeneous broadening is many orders of magnitude larger than P/h and is not particularly sensitive to RF power levels, provided the RF level

remains small compared to the EQI. The interested reader is referred to Callaghan *et al.* (1988) and Back *et al.* (1988) for further details.

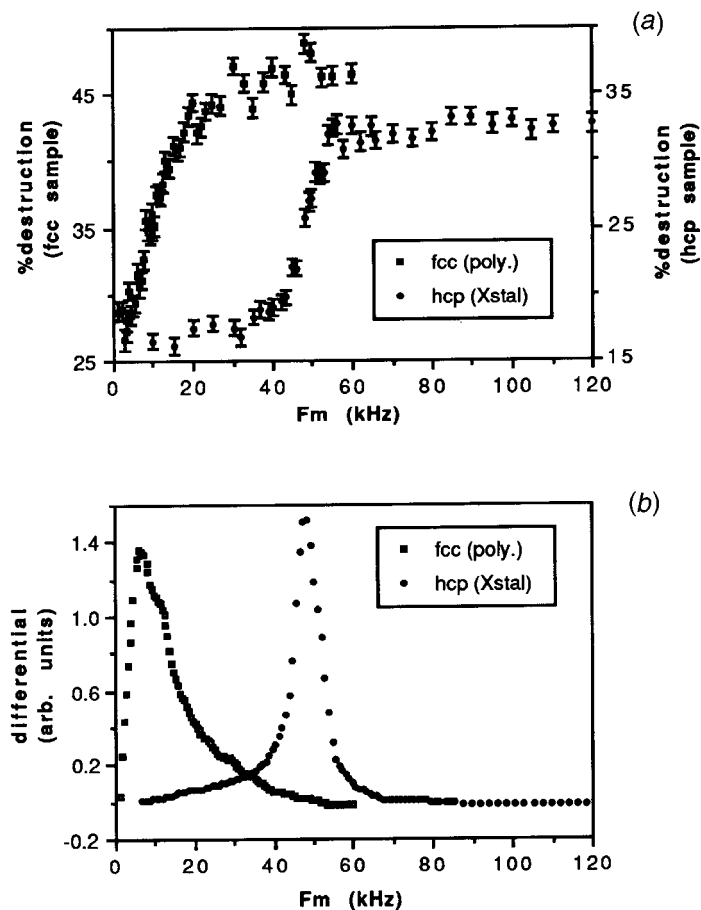


Fig. 7. (a) Raw MAPON data for a $2\ \mu\text{m}$ thick polycrystalline fcc cobalt foil and a $5\ \mu\text{m}$ hcp single crystal, with the detector parallel to the c -axis. In both cases the RF sweep, $d\nu/dt$, was positive and the sweep duration was 147 ms. (b) The analytical differentials of these spectra (after Hutchison *et al.* 1991).

3. CoNi Measurements

This section describes EQI measurements made using MAPON for ^{58}Co and ^{60}Co probes in single crystal nickel, these measurements complementing earlier work for the same probes in Fe (Back *et al.* 1988; Back 1988).

(3a) Experimental Details

For this work $^{58}\text{CoNi}$ and $^{60}\text{CoNi}$ specimens were prepared by thermal diffusion. In each case the activity was loaded onto the electropolished surface of a 1 mm thick, 7 mm dia. nickel single crystal [cut along the (110) plane], from aqueous

solution, dried and then annealed under an atmosphere of 50% hydrogen and 50% argon at 950°C for 45 minutes. After removal from the furnace, the crystal was wiped with ethanol to remove undiffused activity. The remaining specimen activity was 28 μCi for $^{58}\text{CoNi}$ and 22 μCi for $^{60}\text{CoNi}$ respectively. A calculation using Fick's law gives a root mean square diffusion depth of $x_{\text{rms}} \sim 1.5 \mu\text{m}$ assuming a diffusion constant for ^{60}Co into Ni of $D_0 = 1.39 \times 10^{-4} \text{ m}^2 \text{ s}^{-1}$ and activation energy $Q = 275.9 \text{ kJ mol}^{-1}$ (Hassner and Lange 1965). This theoretical diffusion depth is reasonable, given the opposing constraints of good solid substitution versus maintaining the probe atoms near the surface due to RF skin depth considerations.

Each specimen was in turn soldered to the copper cold finger of a ^3He - ^4He dilution refrigerator such that the applied magnetic field and 0° γ -detection direction were along a specified surface crystal direction as previously identified by Laue back reflection. For $^{58}\text{CoNi}$, measurements were made for both easy $\langle 111 \rangle$ and hard $\langle 100 \rangle$ directions, while $^{60}\text{CoNi}$ was mounted along $\langle 111 \rangle$ only. A pair of 12 mm loops of copper wire generated the RF field perpendicular to the applied field and parallel to the specimen surface. All RF power levels specified for the transient techniques were measured as envelope peak to peak voltages (V_{pp}) into a 50Ω load. Temperatures of $\leq 8 \text{ mK}$ were achieved during the NMRON measurements. Two HP Ge detectors were used for γ -ray counting, placed in the 0° and 180° positions, the 811 keV γ -transition being measured for ^{58}Co whilst the sum of the 1.17 and 1.33 MeV lines were used for ^{60}Co .

(3b) EQI Results

Before applying MAPON to the CoNi systems, the normal suite of precursor LTNO and NMRON experiments were performed. A 'magnetisation' curve, i.e. γ -ray anisotropy versus applied field, was produced to determine the applied magnetic field necessary for saturation of each sample in each of the crystalline directions. This was found to be 0.15 T for the easy axis and 0.3 T for the hard axis. Further, the $^{60}\text{CoNi}$ saturated anisotropy was found to be only $\sim 14\%$ compared to the expected 23% at 8 mK. Therefore after EQI determination on this sample it was etched and mounted a second time along the same $\langle 111 \rangle$ direction, yielding marginally larger 16% anisotropy. Both the 'pre-etched' and 'post-etched' results, referred to as $^{60}\text{CoNi}(1)$ and $^{60}\text{CoNi}(2)$, are presented below.

The resonant line shape in the magnetic frequency domain was determined next. Ordinarily this is done with CW NMRON but in the case of $^{58}\text{CoNi}$, the unusually rapid spin-lattice relaxation meant that pulsed FM NMRON (Foster *et al.* 1981) was required to obtain the line shapes, stepping through the resonance with short (ms), fixed amplitude, frequency modulated pulses, interleaved with pulses without FM to define a baseline. Fitting of the resultant lines with Gaussian distributions yielded $\nu_0(0.15 \text{ T}) = 182.50(15) \text{ MHz}$ and $\Gamma_{\text{FWHM}} = 2.2(3) \text{ MHz}$ along $\langle 111 \rangle$ and $\nu_0(0.30 \text{ T}) = 179.90(20) \text{ MHz}$ and $\Gamma_{\text{FWHM}} = 1.8(3) \text{ MHz}$ along $\langle 100 \rangle$. For $^{60}\text{CoNi}$, with the smaller probe nuclear g -factor CW NMRON was successful, see Fig. 2, from which $\nu_0(0.15 \text{ T}) = 68.68(2) \text{ MHz}$ and $\Gamma_{\text{FWHM}} = 0.87(4) \text{ MHz}$ were obtained.

It is then considered useful to perform single passage measurements prior to a MAPON run to investigate adiabatic parameters, non-resonant effects and provide a concise EQI sign determination. Such single passage measurements

were performed on $^{58}\text{CoNi}$ $\langle 111 \rangle$ and $\langle 100 \rangle$ along with $^{60}\text{CoNi}$ $\langle 111 \rangle$, all resulting in a net negative sign for the EQI. This determination then allowed the MAPON measurements to concentrate on sweep-up runs only which in this instance are passages entering the least populated Zeeman states first.

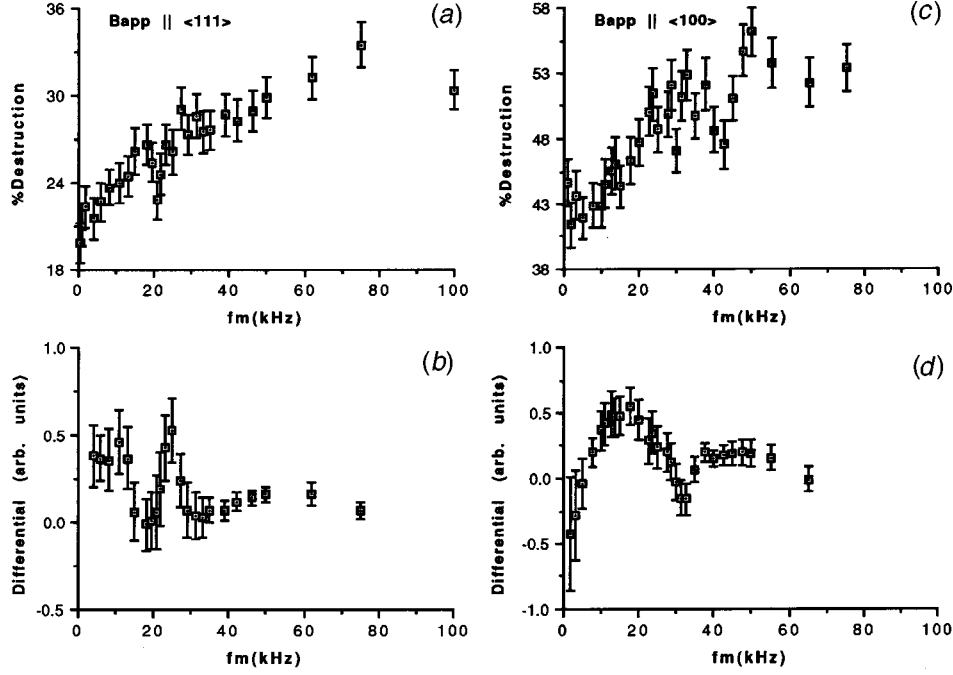


Fig. 8. MAPON spectroscopy applied to $^{58}\text{CoNi}$. Parts (a) and (b) show the raw and differential MAPON spectra respectively obtained with $B_{\text{app}} = 0.15$ T along the easy $\langle 111 \rangle$ direction. Parts (c) and (d) show the raw and differential MAPON spectra respectively obtained with $B_{\text{app}} = 0.30$ T along the $\langle 100 \rangle$ direction.

Raw integral and analytically differentiated MAPON signals versus modulation frequency f_m for $^{58}\text{CoNi}$ along both the $\langle 111 \rangle$ and $\langle 100 \rangle$ directions are shown in Fig. 8. The $\langle 111 \rangle$ integral MAPON data set was recorded by applying an RF voltage of $V_{\text{RF}} = 5.1V_{\text{pp}}$, and a sweep up of duration 147 ms covering ± 1 MHz centred about 182.2 MHz. The integral MAPON data set for $B_{\text{app}} \parallel \langle 111 \rangle$ (Fig. 8a) shows a gradual and more linear rise in signal as f_m is varied from below to above the EQI strength $P/h = 3eQV_{zz}/4I(2I-1)\hbar$ than that obtained for other systems (e.g. Fig. 7). Furthermore there appears to be a clear abrupt effect at 23 kHz as is theoretically predicted (Callaghan *et al.* 1988; Back *et al.* 1988) when the modulation frequency is $f_m = P/h$. Taking the sign of the EQI as negative (refer to earlier single passage determination) the corresponding differential MAPON spectrum, presented in Fig. 8b, indicates a mode value for the EQI of $P/h = -23.0(20)$ kHz with a FWHM of $\Delta P/h = 7.0(10)$ kHz.

The $\langle 100 \rangle$ integral MAPON data set (see Fig. 8c) was recorded by applying an RF voltage of $V_{\text{RF}} = 4.2V_{\text{pp}}$, and a sweep up of duration 147 ms covering ± 1 MHz centred about 179.8 MHz. In spite of a dip and some scatter on the

higher frequency side of the integral data, the differential MAPON spectrum (Fig. 8d) indicates a clear mode value for the EQI of $P/h = -17.5(20)$ kHz with a FWHM of $\Delta P/h = 15.0(20)$ kHz. From these mode P values we find, using the quadrupole moment for ^{58}Co of $Q = +0.22(3)$ b (Raghavan 1989), a value for the EFG at the ^{58}Co site of $V_{zz} = -3.5(4) \times 10^{19}$ V m $^{-2}$ and $V_{zz} = -2.6(3) \times 10^{19}$ V m $^{-2}$ along the $\langle 111 \rangle$ and $\langle 100 \rangle$ directions respectively.

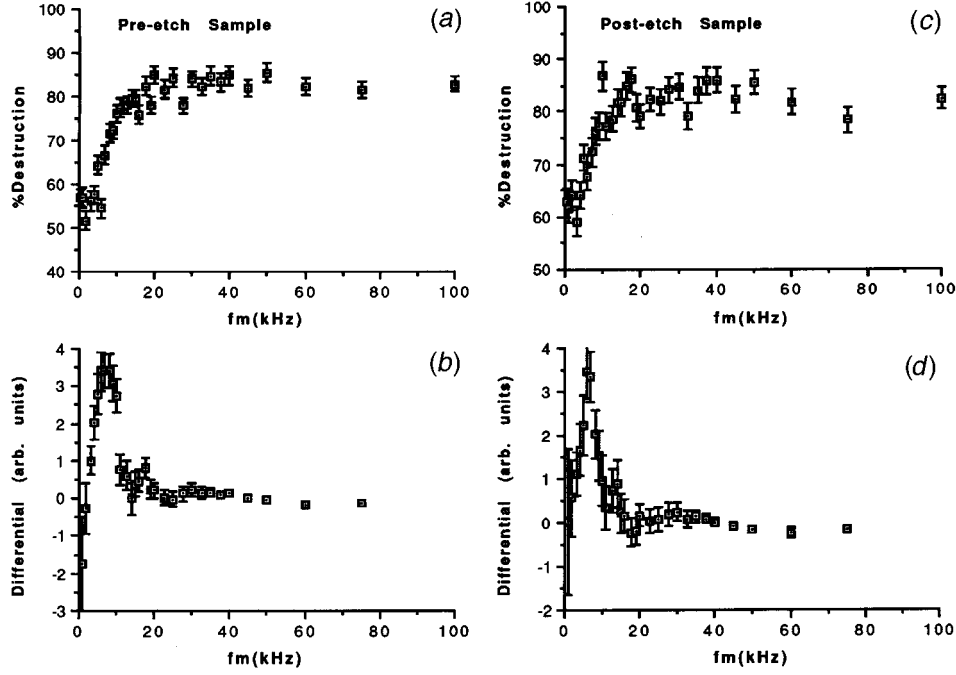


Fig. 9. Sweep up MAPON results for $^{60}\text{CoNi}$ $\langle 111 \rangle$ with $B_{\text{app}} = 0.15$ T, $V_{\text{RF}} = 10.6 V_{\text{pp}}$ in 147 ms and a ± 1 MHz sweep width centred around 68.7 MHz. Parts (a) and (b) show the raw and differential MAPON spectra respectively for $^{60}\text{CoNi}$ (1), while (c) and (d) show the raw and differential MAPON spectra respectively for $^{60}\text{CoNi}$ (2).

In Fig. 9 we show plots of the raw integral and analytically differentiated MAPON signals versus modulation frequency f_m for $^{60}\text{CoNi}$ (1) [parts (a) and (b) respectively] and $^{60}\text{CoNi}$ (2) [parts (c) and (d) respectively] along the $\langle 111 \rangle$ direction. Both integral MAPON data sets were recorded by applying an RF voltage of $V_{\text{RF}} = 10.6 V_{\text{pp}}$, and a sweep up of duration 147 ms covering ± 1 MHz centred about 68.7 MHz. Both show a clear signal transition as f_m is varied from below to above the EQI strength $P/h = 3eQV_{zz}/4I(2I - 1)h$. Taking the sign of the EQI as negative, the corresponding differential MAPON spectra as presented in Figs 9b and 9d indicate mode values for the EQI of $P/h = -6.6(5)$ kHz and $P/h = -6.0(5)$ kHz respectively for the pre-etched and post-etched samples, while both indicated FWHMs of $\Delta P/h = 6.0(5)$ kHz. For these mode P values we find, using the quadrupole moment for ^{60}Co of $Q = +0.44(5)$ b (Raghavan 1989), a value for the EFG at the ^{60}Co site of $V_{zz} = -3.7(3) \times 10^{19}$ V m $^{-2}$ and $V_{zz} = -3.4(3) \times 10^{19}$ V m $^{-2}$ respectively for the pre-etched and post-etched

samples. These EFG values are also in agreement with the above $^{58}\text{CoNi}$ value, along the $\langle 111 \rangle$ direction.

Table 1. EQI mode values \bar{P}/h and FWHM distributions $\Delta P/h$ from MAPON measurements on Mn and Co probes in single crystal iron and nickel

Polycrystalline $^{60}\text{CoFe}$ and $^{60}\text{CoCo}(\text{fcc})$ results are shown for comparison. Mode EFGs derived from the P values are also given

Impurity	Host/Direction	\bar{P}/h (kHz)	$\Delta P/h$ (kHz)	V_{zz} ($10^{-19} \text{ V m}^{-2}$)
^{54}Mn	Fe $\langle 100 \rangle^{(a)}$	$-4.4(4)$	$4.0(5)$	$-1.11(13)$
	Ni $\langle 111 \rangle^{(b)}$	$+3.5(5)$	$4.0(5)$	$+0.88(17)$
	Ni $\langle 100 \rangle^{(b)}$	$+3.5(5)$	$4.2(5)$	$+0.88(17)$
$^{57}\text{Co}^*$	Fe $\langle 100 \rangle^{(c)}$	$+9.0(10)$	$2.5(5)$	$+2.0(5)$
^{58}Co	Fe $\langle 100 \rangle^{(d)}$	$+23.0(30)$	$11.0(10)$	$+3.5(5)$
	Fe $\langle 111 \rangle^{(d)}$	$+7.3(9)^\ddagger$	$8.0(1)$	$+1.1(3)$
	Ni $\langle 111 \rangle^{(e)}$	$-23.0(20)$	$7.0(10)$	$-3.5(4)$
	Ni $\langle 100 \rangle^{(e)}$	$-17.5(20)$	$15.0(20)$	$-2.6(3)$
$^{60}\text{Co}^*$	Fe $\langle 100 \rangle^{(c)}$	$+4.5(10)$	3	$+2.5(6)$
^{60}Co	Fe $\langle 100 \rangle^{(d)}$	$+4.5(10)$	$7.5(5)$	$+2.5(6)$
	Fe $\langle 111 \rangle^{(d)}$	$+2.1(3)^\ddagger$	$4.5(5)$	$+1.2(3)$
	Ni $\langle 111 \rangle^{(e)}$	$-6.3(4)^\#$	$6.0(5)$	$-3.6(3)$
	Fe poly. ^(f)	$+4.5(5)$	$4.0(5)$	$+2.5(5)$
	Co poly. ^(g)	$-6.2(5)$	$12.0(7)$	$-3.5(5)$

* Denotes co-diffused sample.

‡ Averaged result for measurements at different B_{app} .

$^\#$ Averaged result for pre-etched and post-etched sample.

(a) Yazidjoglou *et al.* (1994). (b) Chaplin *et al.* (1988). (c) Back *et al.* (1989). (d) Back *et al.* (1988); Back (1988). (e) This work. (f) Unpublished, tabulated in Chaplin and Hutchison (1992). (g) Hutchison *et al.* (1991, 1992a).

4. Discussion

Table 1 presents measured EQI (\bar{P}/h) and deduced EFG (V_{zz}) results for the 3d impurities in Fe and Ni obtained by MAPON spectroscopy on isotopes whose nuclear quadrupole moment (sign and magnitude) is well-established by independent measurements. In all cases the \bar{P}/h value quoted is obtained from the maximum in the MAPON differential; the errors quoted reflect, in the main, the uncertainty in selecting this maximum in the well-resolved frequency distribution of EQIs, rather than the fundamental frequency resolution limit in the MAPON technique. This latter constraint is typically 200 Hz in the experiments performed in Canberra using carefully selected, low noise double balance mixers. For the derived V_{zz} values the accuracy of the relevant quadrupole moment Q (Raghavan 1989) is also accounted for in the stated error. Included in Table 1 are the Oxford $^{57,60}\text{CoFe}$ $\langle 100 \rangle$ results (Back 1988; Back *et al.* 1989) and in addition, for comparison, two Canberra MAPON results on polycrystalline $^{60}\text{CoFe}$ and $^{60}\text{CoCo}(\text{fcc})$. Magnetic field independence of the single crystal EFGs along a given principal crystal axis in the host saturation region have previously been demonstrated (Back 1988; Chaplin and Hutchison 1992). More recently Seewald *et al.* (1997) have confirmed this observation for single crystal $^{188}\text{IrFe}$ and as a

consequence no applied field values are quoted. For the CoFe system, applied magnetic field independence to 2 T (Back *et al.* 1988) and for the 5sp system SbFe field independence to 5 T (Chaplin *et al.* 1988) have been observed. For such small EQI splittings a field dependence would occur for second order magnetic interactions, e.g. pseudo-quadrupole effects.

The widths of the EFG distributions ($\Delta P/h$) in Table 1 are FWHMs taken from the MAPON differentials. The site selective MAPON process, with appropriately narrow frequency sweeps, picks out those impurity nuclei with the correct magnetic hyperfine field rejecting those that are in 'bad' sites (i.e. sites which generally reduce the integral gamma anisotropy). However, as is apparent from the $\Delta P/h$ listed in Table 1, the 'good' sites can still carry a relatively wide range of EQI frequencies which the MAPON technique readily resolves. Likely causes of such variations are impurity effects and host lattice inhomogeneities such as defects and dislocations. In particular, asymmetric concentration broadening can be observed in lightly diffused alloys especially if the activity (e.g. ^{60}Co) is not carrier-free. This is not a fundamental limitation for such thermally prepared NMRON samples as the symmetric EQI distributions for $^{60}\text{CoNi}$ in Fig. 9 illustrate. Also, Back (1988) obtained the same mode values for $^{60}\text{CoFe}$ (100) in two different samples of significantly different concentration, leading to widely differing broadenings (see Table 1). This relative robustness of the impurity mode EFG on Co impurities in single crystal Fe, despite concentration broadening effects, strongly suggests a dominant localised contribution to the EFG. A useful figure-of-merit to compare the quality of impurity systems is $F = \bar{P}/\Delta P$. The asymptotic upper limit in the 3d series towards which the best impurity systems might aspire is the pure elemental case $^{60}\text{CoCo}$ (hcp) of Fig. 7 (Hutchison *et al.* 1991) with $F = 6.6(7)$.

From Table 1 the weighted average for all listed Co isotopes in single crystal Fe, along $\langle 100 \rangle$ is $V_{zz} = +2.6(3) \times 10^{19} \text{ V m}^{-2}$. This may be contrasted with the recent MAPON result on $^{188}\text{IrFe}$ $\langle 100 \rangle$ of $V_{zz} = -39.4(6) \times 10^{19} \text{ V m}^{-2}$ (Seewald *et al.* 1997). From nuclear quadrupole systematics the signs of the respective quadrupole moments leading to these opposing signs in EFGs are indisputable (Seewald *et al.* 1996; Niesen and Huiskamp 1972). In this respect it is worth mentioning that, at the time the basic origins of the 5d impurity EFGs (e.g. Ir) in Fe and Ni were first being investigated theoretically (Gehring and Williams 1974; Demangeat 1974, 1975; Aiga and Itoh 1974), the sign of the EQI for $^{192}\text{IrNi}$ (single crystal) was erroneously assigned as positive (Johnston and Stone 1972). In addition, two groups (Gehring and Williams 1974; Aiga and Itoh 1974) were strongly influenced in their calculations by the apparent isotropy of the EQI (EFG) in single crystals, from CW NMRON on $^{192}\text{IrNi}$ (Johnston and Stone 1972) and from spin echo on 0.3 at% $^{193}\text{IrFe}$ (Aiga and Itoh 1974). The latter experimental result has recently been shown to be not reproduced in the extreme dilution limit in the MAPON experiment on $^{188}\text{IrFe}$ (Seewald *et al.* 1997). Instead, there is an 80% increase (without sign change) from $\langle 111 \rangle$ to $\langle 100 \rangle$, to be compared with a $\sim 200\%$ increase (without sign change) for the EQIs in $^{58}\text{CoFe}$. The failure to observe EFG anisotropy in the spin echo $^{193}\text{IrFe}$ experiment is almost certainly due to the excessive impurity concentration. Subsequent to this initial and confused flurry of activity in the early seventies the correct signs for the EQIs began to emerge, primarily from the Munich group and commencing with $^{192}\text{IrNi}$, Fe where the hosts were polycrystalline (Hagn *et al.* 1979, 1980).

When Co is placed in Ni, in comparison to Co in Fe, the following observations from Table 1 prevail:

- (1) The absolute magnitudes of the EFGs are not very different, certainly along the magnetic easy axes $\langle 111 \rangle$ for Ni, $\langle 100 \rangle$ for Fe.
- (2) The EFG sign in Ni is opposite to Fe along all principal directions.
- (3) The anisotropy between magnetically easy and hard axes is evident but significantly reduced. This result is seen by reference to the ^{58}Co probe.

Observation (3) implies that the EFG result for polycrystalline CoNi should not be too different to CoNi $\langle 111 \rangle$. In turn, one expects the same sign and magnitude EFG as for CoCo(fcc) since the lattice constants differ between fcc Ni and fcc Co by $\sim 1\%$, and this is indeed observed (Table 1). This Co impurity EFG is remarkably sensitive to crystal field effects (crystal symmetry and lattice constant), providing opposite signs in the bcc Fe host versus fcc Ni and Co.

The same comparison can be made for Ir in Ni versus Ir in Fe, by recourse to the literature. Here the much larger EFGs, an order of magnitude larger than the Co probe, can allow frequency resolution in CW NMRON, known as QI NMRON for favourable low-spin probe nuclei. Completely resolved quadrupole sub-resonances were first seen in $^{199}\text{AuFe}$ (Callaghan *et al.* 1976) and for the ^{192}Ir probe, a direct relevance to this paper, by Hagn *et al.* (1979, 1980) in Fe and Ni polycrystalline hosts:

- (1) The inferred EFG in the Ni host is approximately one half that in Fe (Hagn *et al.* 1979, 1980; Seewald *et al.* 1997).
- (2) The signs of the EFGs are the same in the two hosts, namely negative (Hagn *et al.* 1979, 1980).
- (3) The anisotropy between magnetically easy and hard axes is prominent in Fe (Seewald *et al.* 1997) but not as strong as for CoFe (above 80% versus 200%). The anisotropy for IrNi has not been measured with MAPON precision to date but Johnston and Stone (1972) estimated isotropy to within 10% from poorly resolved QI NMRON.

The lack of a reversal of the sign of the EFG for the 5d impurity, Ir in changing from Ni to Fe hosts, is in striking contrast to the 3d impurity, Co. For the 5d impurity, spin-orbit coupling dominates. Following Gehring and Williams (1974) or Aiga and Itoh (1974), one assumes that the Ir impurity carries no orbital angular momentum in a paramagnetic host, the ferromagnetic host acts on the impurity spin and through strong impurity spin-orbit coupling, the orbital moment aligns with the direction of the internal fields as determined by the electronic magnetisation. The EFG is isotropic when all five electronic sub-bands contribute to the impurity-host interaction. Demangeat (1974, 1975) undertook a more sophisticated, Ni host specific calculation. He again invoked strong impurity spin-orbit coupling but was led to anisotropy in the EFG through virtual bound state (VBS) theory, wherein equivalence between the host spin bands is immediately lost as Ir presents a charge 'excess' of -1 relative to Ni leading to ~ 0.9 holes per iridium impurity in the spin up d-band. The essential difference between the two approaches is that the first assumes a local d-spin impurity that induces an orbital moment through spin-orbit coupling and crystal field effects are considered secondary (actually *assumed* negligible due to the experimental

results of that era favouring isotropic EFGs). The second VBS approach requires no local moment, a priori, but does require more detailed knowledge of impurity charge effects on the specific band structure of the host. Both require the strong spin-orbit coupling of the impurity, but omit the weaker spin-orbit coupling of the host atoms.

For the 3d impurity Co there is an entirely different approach, to which we are led by the results of the 3d, 5d impurity EFG comparisons between cubic Fe and Ni. In comparison to magnetic hyperfine fields of the nd transition metal impurities in Fe and Ni, there is a gross simplification. When dealing with EFGs in cubic metals there is no host conduction electron polarisation analogue which may modify local impurity moment contributions, or in *ab initio* calculations (Akai *et al.* 1990), lead more directly to impurity magnetic hyperfine fields through s-d hybridisation. Let us postulate that the Co impurity in the paramagnetic host, in contrast to the 5d impurity in a paramagnetic host carries significant unquenched orbital angular momentum. The underlying failure for complete quenching is, fundamentally, the particularly strong orbital character of the free ion Co wave functions, relative to its immediate neighbours Fe and Ni. In the ferromagnetic hosts, in the language of local moment states, the width of the local d-state is insufficiently narrow to force a pure spin moment. The spin-orbit coupling is a negligible consideration in inducing an orbital moment, it is already there on the Co impurity, with connotations of a spatially more extended influence than spin only magnetism. Evidence in the literature for such an intrinsic residual unquenched orbital angular momentum on the isolated Co impurity in metals is abundant:

- (1) Co as a very dilute impurity in Cu has an anomalously large positive Knight shift (KS). It is even larger in Au, but a high Kondo temperature in Ag obscures any further evidence (Brewer 1986).
- (2) Co as a very dilute impurity in Pd has a positive hyperfine field (Brewer 1986). Pd is almost a band ferromagnet, exhibiting a large negative KS in the pure element (Carter *et al.* 1976), and is that transition metal host closest in magnetic character to Fe and Ni without being ferromagnetic. Co has a propensity to induce moments on its immediate surrounds in Pd and Pt.
- (3) Unlike the other group members Rh and Ir, Co is not at the peak of the eyeball curve in the right hand series of nd magnetic hyperfine fields in Fe (Stone 1986). This may be viewed as Co being held down relative to Fe on its left and Ni on its right by a sizeable orbital magnetic hyperfine field which is positive. To elevate Co to be at the peak, thereby qualitatively matching Rh and Ir, a minimum orbital field of 5 T is required for the system **CoFe**.
- (4) Co as a dilute impurity in Fe exhibits a positive KS of 1.5% (Foster *et al.* 1981; Yazidjoglou *et al.* 1993), significantly larger than Cu metal of $\sim +0.25\%$. This may also be compared with the KS in the pure ferromagnetic elements $^{59}\text{CoCo}(\text{hcp})+1.94(25)\%$ (Fekete *et al.* 1976); $^{57}\text{FeFe}+0.78(10)\%$ (Oppelt *et al.* 1980); and $^{61}\text{NiNi}+0.90(27)\%$ (Kropp *et al.* 1982).

Postulating a significant orbital moment on the Co ion in Fe and Ni without the intermediary of spin-orbit coupling implies immediately enhanced sensitivity to crystal field effects, relative to Ir. The implication of the EFG changing sign from negative for Ir in Fe, to positive for Co in Fe, is that there are (at least) two competing mechanisms on orienting unquenched orbital angular momentum. For the 5d impurity it is dominated by impurity spin-orbit coupling and hence the electronic magnetisation; for the 3d impurity it is dominated by crystal field effects and the role of the impurity spin-orbit coupling is secondary in comparison. Since these competitive effects lead to a sign change in EFG (**CoFe** $\langle 100 \rangle$ is positive and **IrFe** $\langle 100 \rangle$ is negative), by interpolation the prospects of a well-defined orientation of any unquenched orbital angular momentum on the 4d impurity, Rh, are not strong. To date there have been no MAPON measurements on **RhFe** alloys; however, Ohya *et al.* (1990) have examined single crystal $^{106}\text{RhNi}$ with single passage and MAPON. They found a very small EQI extremely broadly distributed, whose inferred EFG magnitude is significantly less than for **CoFe** and **CoNi**. Given that ^{106}Rh ($I = 1$) has a quadrupole moment Q , likely to be of order 0.1–0.5 b, it is most surprising that the $^{106}\text{RhNi}$ system exhibited no well-defined EFG, in striking contrast to the ^{58}Co [$I = 2$ and $Q = 0.22(3)$ b] impurity probe with its smaller effective quadrupole moment $Q/4I(2I - 1)$. This is powerful empirical evidence that the above competitive processes lead to a nulling, certainly with respect to net orientation, and possibly with respect to magnitude of the impurity EFG for Rh in Ni.

To distinguish between the theoretical model of Demangeat (1974, 1975) and that of Gehring and Williams (1974) and Aiga and Itoh (1974), $^{188}\text{IrNi}$ single crystal MAPON studies would be fruitful. No anisotropy in the EFG supports the local moment, minimal crystal field effect approach of the latter authors. (Demangeat's calculations lead to a strong anisotropy for **IrNi**.) MAPON spectroscopy is easily capable of resolving this question well below the 10% limits on isotropy currently in the literature (Johnston and Stone 1972). $^{188}\text{IrCo}$ (fcc) is another case of considerable interest where the host will necessarily be polycrystalline. Comparison with the above-mentioned $^{188}\text{IrNi}$ study should show whether or not the EFGs are host band dependent or crystal field effects are in fact important in determining the EFG in magnitude or orientation.

In contrast to **CoFe** and **CoNi**, it is abundantly clear from Table 1 that Mn impurities do not carry significant unquenched orbital angular momentum. From the limited systematics available one expects the EFG for **MnFe** $\langle 111 \rangle$ to be negative and $\sim 1 \times 10^{19} \text{ V m}^{-2}$. The complete absence of orbital angular momentum for this impurity is to be expected, from Hund's rules, and hence the insensitivity to principal crystal field directions in a given host is entirely expected. Both **MnFe** (Yazidjoglou *et al.* 1994; Seewald *et al.* 1995) and **MnNi** (Yazidjoglou *et al.* 1988; Seewald *et al.* 1995) yield a zero Knight shift. The change of EFG sign from Fe to Ni hosts is, however, quite unexpected. Apart from the missing $^{54}\text{MnFe}$ $\langle 111 \rangle$ measurement, $^{54}\text{MnCo}$ (fcc) would be a useful addition to provide insight to the basic mechanisms responsible.

In summary, we have demonstrated how EFG measurements at Co nuclei in single crystal Ni have assisted in unravelling mechanisms responsible for the unquenched orbital angular momentum at impurity probes, Co, Rh, Ir in

ferromagnetic Fe and Ni. It is argued that even in this limited group there are two competitive mechanisms at play:

- (i) An inherent unquenched orbital angular momentum on the Co impurity, which is predominantly sensitive to crystal field effects as the dominant orientational interaction. The implication is that there is a significant positive orbital hyperfine field on the Co impurity. Since this orbital field is presumably locked to crystal field directions, relative to other hyperfine field contributions in the 3d series, fluctuations in this orbital component will be suppressed. This should lead to a local minimum in the nuclear spin lattice relaxation rate for Co in Fe relative to its immediate neighbours Fe and Ni. This has recently been observed (Beck *et al.* 1998, present issue p. 267).
- (ii) An extrinsic, induced orbital angular momentum on the Ir probe, from impurity spin-orbit coupling, which is inherently less sensitive to crystal field effects, and more sensitive to spin orientation as defined by domain magnetisation.

In Fe hosts which are currently the better studied, in single crystal form, there is a change in sign of EFG from 3d Co to 5d Ir; positive to negative. A corollary, therefore, is that the 4d impurity Rh in Fe will most likely interpolate as exhibiting very weak orientational effects on any EFG arising from unquenched orbital angular momentum, if indeed there is any local moment EFG present. In this respect a MAPON study of $^{106}\text{RhFe}$ single crystals specifically along the $\langle 100 \rangle$ direction, is a very high priority. We note that Seewald *et al.* (1995) have resonated $^{99\text{m},101\text{m}}\text{Rh}$ and $^{52}\text{MnFe}$ in a careful but limited field shift study which led to the conclusion of no Knight shift within the accuracy of the nuclear magnetic moments, thereby removing several long standing puzzles in the literature (see Yazidjoglou *et al.* 1993). However, while this is encouraging, these measurements need to be extended to fields significantly higher before the current null result for RhFe can be accepted as supporting evidence for the above RhFe conjecture.

Finally, it is pointed out that the signs of the EFGs are now unequivocal for both 3d (Co) and 5d (Ir) impurities and this should give the theoreticians valuable new constraints on their model calculations.

Acknowledgments

The authors wish to thank Dr Glen Stewart for reading the manuscript and Dr Stephen Harker for assistance with diagrams. This work was supported by an Australian Research Council grant.

References

- Aiga, M., and Itoh, J. (1974). *J. Phys. Soc. Jpn* **37**, 967.
 Akai, H., Akai, M., Blügel, S., Drittler, B., Ebert, H., Terakura, K., Zeller, R., and Dederichs, P.H. (1990). *Prog. Theor. Phys. Suppl.* **101**, 11.
 Back, P.J. (1988). *Hyperfine Interact.* **43**, 211.
 Back, P.J., Callaghan, P.T., and Chaplin, D.H. (1988). *Phys. Rev. B* **37**, 4911.
 Back, P.J., Nawaz, Z., and Stone, N.J. (1989). *Hyperfine Interact.* **51**, 909.
 Beck, E., Brewer, W.D., Funk, T., and Klein, E. (1998). *Aust. J. Phys.*, **51**, 267.
 Brewer, W.D. (1986). In 'Low Temperature Nuclear Orientation' (Eds N.J. Stone and H. Postma), Ch. 9 (North Holland: Amsterdam).
 Callaghan, P.T., Johnston, P.D., and Stone, N.J. (1974). *J. Phys. C* **7**, 3161.

- Callaghan, P.T., Lattimer, W.M., Johnston, P.D., and Stone, N.J. (1976). *Hyperfine Interact.* **2**, 288.
- Callaghan, P.T., Back, P.J., Chaplin, D.H., Foster, H.R., and Wilson, G.V.H. (1985). *Hyperfine Interact.* **22**, 39.
- Callaghan, P.T., Back, P.J., and Chaplin, D.H. (1988). *Phys. Rev. B* **37**, 4900.
- Carter, G.C., Bennett, L.H., and Kahan, D.J. (1976). *Prog. Mater. Sci.* **20**, 289.
- Chaplin, D.H., and Hutchison, W.D. (1992). *Hyperfine Interact.* **75**, 209.
- Chaplin, D.H., and Wilson, G.V.H. (1986). In 'Low Temperature Nuclear Orientation' (Eds N.J. Stone and H. Postma), Ch. 14 (North Holland: Amsterdam).
- Chaplin, D.H., Hutchison, W.D., Kopp, M.P., and Yazidjoglou, N. (1988). *Hyperfine Interact.* **43**, 241.
- Demangeat, C. (1974). *J. Phys. F* **4**, L64.
- Demangeat, C. (1975). *J. Phys. F* **5**, 169.
- Don, C.G. (1972). Single passage NMR on oriented nuclei. PhD Thesis, Monash University.
- Fekete, D., Grayevsky, A., Shaltiel, D., Goebel, U., Dormann, E., and Kaplan, N. (1976). *Phys. Rev. Lett.* **36**, 1566.
- Fekete, D., Boasson, H., Grayevski, A., Zevin, V., and Kaplan, N. (1978). *Phys. Rev. B* **17**, 355.
- Foster, H.R., Chaplin, D.H., Swan, D.E., Turrell, B.G., and Wilson, G.V.H. (1981). *Hyperfine Interact.* **10**, 1149.
- Gehring, G.A., and Williams, H.C.L. (1974). *J. Phys. F* **4**, 291.
- Hagn, E. (1996). *Hyperfine Interact.* **97/98**, 409.
- Hagn, E., Lenthold, K., Zech, E., and Ernst, H. (1979). *Phys. Lett. A* **58**, 32.
- Hagn, E., Lenthold, K., Zech, E., and Ernst, H. (1980). *Z. Phys. A* **295**, 385.
- Hasser, A., and Lange, W. (1965). *Phys. Status Solidi* **8**, 77.
- Herzog, P. (1996). Personal communication.
- Hinfurtner, B., Hagn, E., Zech, E., and Eder, R. (1991). *Phys. Rev. Lett.* **67**, 812.
- Hutchison, W.D., Edge, A.V.J., Yazidjoglou, N., and Chaplin, D.H. (1991). *Phys. Rev. Lett.* **67**, 3436.
- Hutchison, W.D., Edge, A.V.J., Yazidjoglou, N., and Chaplin, D.H. (1992a). *Hyperfine Interact.* **75**, 291.
- Hutchison, W.D., Yazidjoglou, N., and Chaplin, D.H. (1992b). *Hyperfine Interact.* **75**, 253.
- Johnston, P.D., and Stone, N.J. (1972). *J. Phys. C* **5**, L303.
- Kropp, H., Dormann, E., Grayevsky, A., and Kaplan, N. (1982). *Solid State Commun.* **44**, 1109.
- Matthias, E., and Holliday, R.J. (1966). *Phys. Rev. Lett.* **17**, 893.
- Niesen, L., and Huiskamp, W.J. (1972). *Physica* **57**, 1.
- Ohya, S., Ashworth, C.J., Nawaz, Z., Stone, N.J., and Back, P.J. (1990). *Phys. Rev. C* **41**, 243.
- Oppelt, A., Fekete, D., and Kaplan, N. (1980). *J. Mag. Magn. Mater.* **15-18**, 660.
- Raghavan, P. (1989). *Atomic Data Nucl. Data Tables* **42**, 189.
- Seewald, G., Hagn, E., Hinfurtner, B., and Zech, E. (1995). *Phys. Rev. B* **51**, 11484.
- Seewald, G., Hagn, E., Hinfurtner, B., Zech, E., Ferkel-Wirth, D., and Eder, R. (1996). *Phys. Rev. Lett.* **77**, 5016.
- Seewald, G., Hagn, E., Zech, E., Ferkel-Worth, D., Burchard, A., and ISOLDE Collaboration (1997). *Phys. Rev. Lett.* **78**, 1795.
- Stone, N.J. (1986). In 'Low Temperature Nuclear Orientation' (Eds N.J. Stone and H. Postma), Ch. 8 (North Holland: Amsterdam).
- Yazidjoglou, N. (1989). An NMRON investigation of electric quadrupole interactions and Knight shifts of dilute impurities in single crystal iron and nickel. PhD Thesis, University of New South Wales.
- Yazidjoglou, N., Chaplin, D.H., Foster, H.R., and Hutchison, W.D. (1988). *Hyperfine Interact.* **43**, 231.
- Yazidjoglou, N., Hutchison, W.D., and Chaplin, D.H. (1993). *J. Phys. C* **5**, 129.
- Yazidjoglou, N., Hutchison, W.D., and Stewart, G.A. (1994). *J. Phys. C* **6**, 7109.